Disclaimer

This note has not been internally reviewed by the DØ Collaboration. Results or plots contained in this note were only intended for internal documentation by the authors of the note and they are not approved as scientific results by either the authors or the DØ Collaboration. All approved scientific results of the DØ Collaboration have been published as internally reviewed Conference Notes or in peer reviewed journals.

DØ Note 2623

Measurement of W and Z p_T Distributions at the Tevatron

Danilo L. Pušeljić

Lawrence Berkeley Laboratory, Berkeley, CA 94720

The measurements of W and Z boson differential cross sections $d\sigma/dp_T$ at the Tevatron are examined. The measurement technique is illustrated with DØ data, and a comparison of smeared theory to data is presented. The performance of an unfolding detector smearing technique based on Bayes' Theorem is demonstrated.

INTRODUCTION

The transverse momentum of intermediate vector bosons (IVB's) produced in proton-antiproton collisions is provided by an initial state gluon radiation. In the low transverse momentum region ($p_T(W,Z) < 20$ GeV/c) multiple soft gluon emission is expected to dominate the initial state radiation and the production cross section of IVB's is calculated using a soft gluon resummation technique (1-5). In the high p_T regime ($p_T(W,Z) > 20$ GeV/c) the cross section is expected to be well described by perturbative QCD calculations (6). Thus a measurement of the transverse momentum distributions may be used to constrain the resummation calculations in the low p_T range and to test the perturbative QCD predictions at high p_T. Deviations from the prediction at large p_T could be an indication of new physics. A good understanding of the $p_T(W)$ distribution is necessary for a precise measurement of the W mass.

The higher center of mass energy available at the Tevatron enables measurements to be extended to larger p_T's than previously measured at the CERN $p\bar{p}$ collider (7). The large W/Z data samples accumulated by DØ and CDF during the 1992-93 and 1994-95 runs will significantly improve the precision with which this quantity is presently known (8). This report describes the measurement technique, presents a comparison of smeared theoretical predictions to DØ data, and discusses an unbiased way to unfold the detector smearing.

MEASUREMENT DESCRIPTION

The measurement of vector boson $d\sigma/dp_T$ differential cross section consists of three basic steps: data selection, background estimation and subtraction, and unfolding of detector smearing. We illustrate these steps for $W \rightarrow e\nu$, and $Z \rightarrow ee$ data samples accumulated with the DØ detector (9) during the 1992-93 Fermilab Tevatron $p\bar{p}$ collider run at $\sqrt{s} = 1.8$ TeV.

Data Selection

Electrons were detected in hermetic , uranium liquid argon calorimeters (10,11), with energy resolution of about $15\%/\sqrt{E(\mathrm{GeV})}$. The $W \rightarrow e\nu$, and $Z \rightarrow ee$ analyses accepted electrons in the pseudorapidity range: $\mid \eta \mid < 1.1$ and $1.5 < \mid \eta \mid < 2.5$. Both analyses used the same trigger which required a

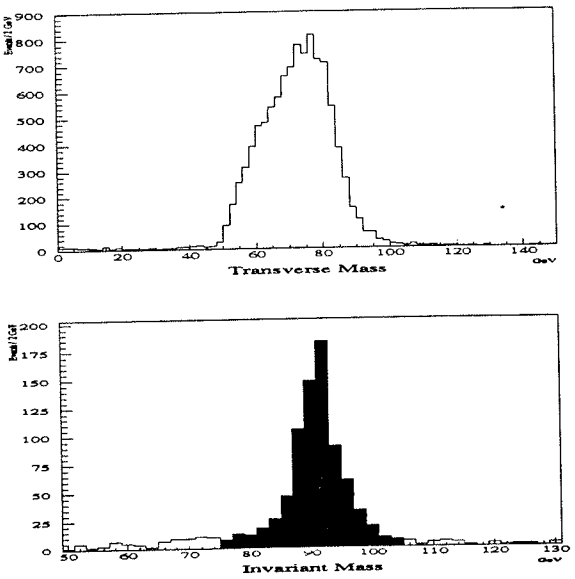

FIG. 1. Transverse mass (top) and invariant mass (bottom) distributions of $W \rightarrow e\nu$ and $Z \rightarrow e^+e^-$ data samples.

single electron with transverse energy (E_T) greater than 20 GeV. Kinematic selections made in the offline analysis required Z boson candidates to have two electrons, each with $E_T > 25$ GeV and W boson candidates to have one electron with $E_T > 25$ GeV and missing transverse energy ($\not\!\!E_T$) greater than 25 GeV. The offline *loose* electron identification consisted of the following requirements: *i*) fraction of energy deposited by the electron in the electromagnetic part of the calorimeter to be greater than 95%; *ii*) transverse and longitudinal shower shapes had to be consistent with those expected for an electron; *iii*) electron had to be isolated with $I < 0.1$. The isolation variable is defined as $I = (E(0.4) - EM(0.2))/EM(0.2)$, where $E(0.4)$ is the total calorimeter energy inside a cone of radius $\sqrt{\Delta\eta^2 + \Delta\phi^2} = 0.4$ and $EM(0.2)$ is the electromagnetic energy inside a cone of 0.2. A *tight* electron satisfied the above *loose* electron criteria and in addition was required to have a good match between the reconstructed track in the central drift chamber (CDC) and the shower centroid in the calorimeter. The W boson candidates were required to have a single *tight* electron, while Z boson candidates were to have at least one *tight* and one *loose* electron. For the $Z \rightarrow e^+e^-$ analysis

events with an invariant mass in the range $75-105$ GeV/c^2 were used. Fig. 1 shows the transverse and invariant mass distributions for W and Z events respectively obtained from 12.8 pb^{-1} of DØ data.

Backgrounds

The measurement of the differential cross section $d\sigma/dp_T$ requires the knowledge of the total amount of background in the sample as well as it's shape as a function of the boson p_T. The dominant source of background in the $Z \rightarrow e^+e^-$ sample is multijet events where two jets have been misidentified as electrons or dircet photon events where jet and photon are identifed as electrons. The amount of multijet background is estimated by performing a fit to the data using the predicted Z boson mass distribution and the experimentally determined shape of the multijet background from dijet and direct photon events.

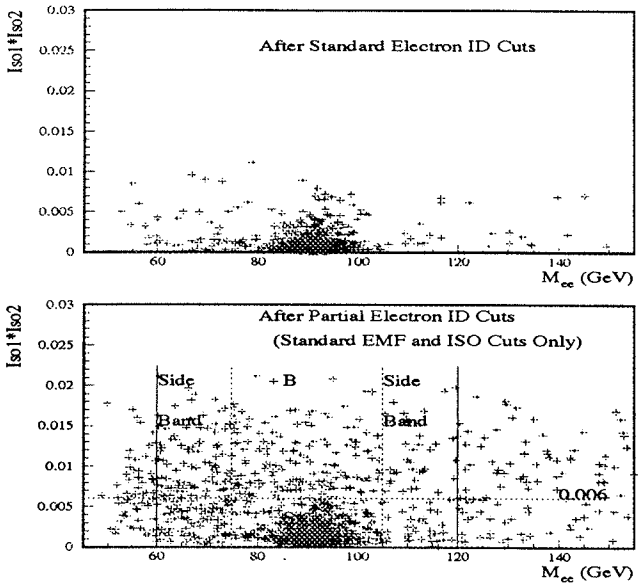

FIG. 2. Product of isolation variables of the two Z boson electrons versus invariant mass, for standard cuts (top) and less stringent electron identification (bottom).

The shape of the multijet background as a function of the Z boson p_T is obtained (12) from data by studying the product of the isolation variables of the two electrons as a function of the e^+e^- invariant mass, shown in Fig. 2 for standard and looser electron identification. The events from region B ($75 < M_{ee} < 105$ GeV/c^2, and $iso1 * iso2 > 0.006$), marked in Fig. 2, were used to parametrize the shape of the multijet background. The distribution obtained is shown in Fig. 3.

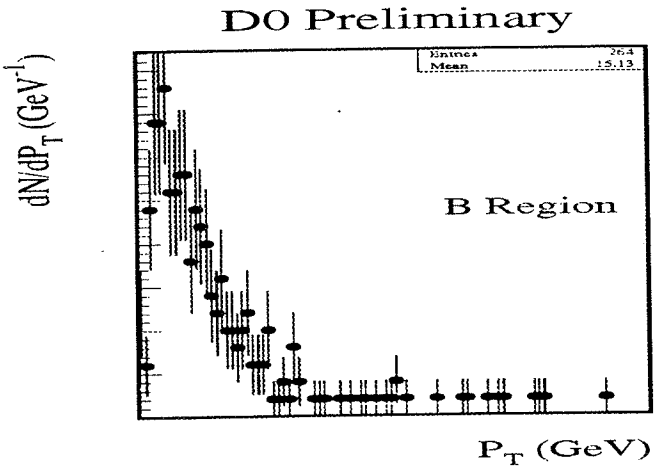

FIG. 3. The shape of the multijet background as a function of the Z boson p_T for the B region of Fig. 2.

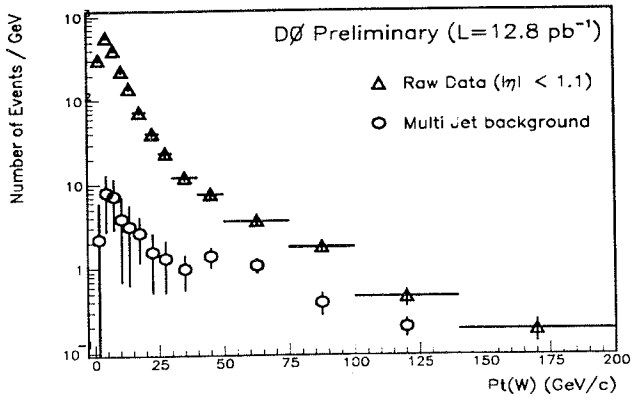

FIG. 4. Raw W p_T distribution (triangles) with multijet background (circles) superimposed.

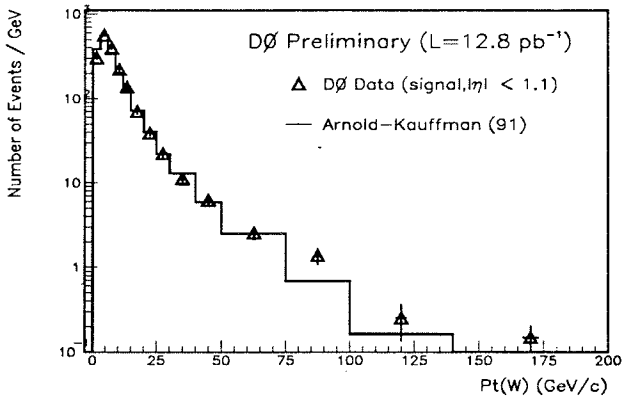

FIG. 5. Multijet background subtracted W p_T distribution of DØ data for $|\eta| < 1.1$ (triangles) with smeared theoretical prediction (histogram) by (4) superimposed.

TABLE 1. Event yields and background estimates for W and Z boson samples

Channel	$W \to e\nu$	$Z \to e^+e^-$
N_{obs}	10338	775
Backgrounds(%):		
$Z \to e^+e^-$	0.6 ± 0.1	-
$W \to \tau\nu$	1.8 ± 0.1	-
Multijet	3.3 ± 0.5	2.8 ± 1.4
Drell-Yan	-	1.2 ± 0.1
Total Bkg (%)	5.7 ± 0.4	4.0 ± 1.4
$\int \mathcal{L}dt(pb^{-1})$	12.8 ± 0.7	12.8 ± 0.7

The dominant sources of background in the $W \to e\nu$ sample are: *i)* multijet events where a jet has been misidentified as an electron; *ii)* $W \to \tau\nu \to e\nu$ decay, and *iii)* $Z \to e^+e^-$ where one of the electrons has been lost. The total multijet background estimate was derived from data by measuring the tail of the $\not\!\!E_T$ distribution of the background and normalizing this at small $\not\!\!E_T$ to the $\not\!\!E_T$ spectrum of the signal sample without the $\not\!\!E_T$ cut imposed. The corresponding shape as a function of $p_T(W)$ is obtained by subtracting the $p_T(W)$ distribution obtained for a set of very clean electron identification cuts from a p_T distribution of background rich sample while accounting for the relative efficiency loss between the two cuts. Fig. 4 shows the obtained distribution superimposed on the raw $p_T(W)$ distribution.

The multijet background subtracted p_T distributions of the W and Z bosons with theoretical predictions smeared by detector resolutions superimposed, are shown in Fig. 5 and Fig. 6. Table 1 summarizes the event yields and background estimates for W and Z samples.

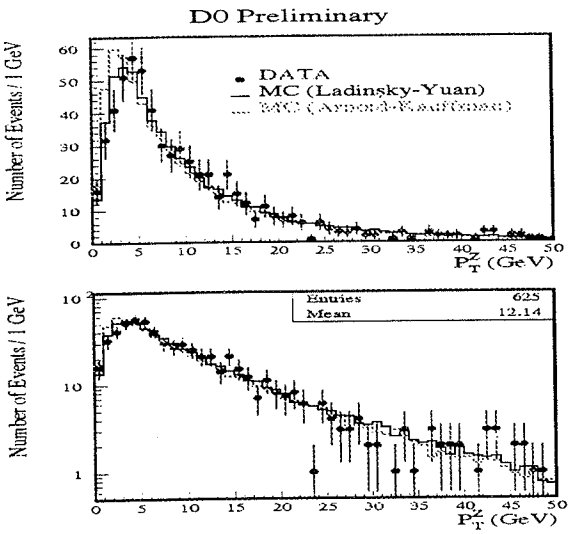

FIG. 6. Multijet background subtracted Z p_T distribution (solid dots) with smeared theoretical predictions by (4) (gray histogram) and (5) (dark histogram) superimposed. Top plot: linear scale; Bottom plot: logarithmic scale.

Unfolding Detector Smearing

In the measurement process true distributions are distorted due to finite detector resolution, limited acceptance and presence of scale that relates measured to true values. We examine a rather elegant and straightforward technique to unfold the smeared distributions based on Bayes' Theorem (13). If one knows the initial probability $P(C_i)$ to have a cause C_i and a conditional probability $P(E_j \mid C_i)$ that cause C_i produced effect E_j then the probability that an observed effect E_j is due to cause C_i is given by:

$$P(C_i \mid E_j) = \frac{P(E_j \mid C_i) \times P(C_i)}{\sum_{k=1}^{n_c} P(E_j \mid C_k) \times P(C_k)} \tag{1}$$

and the best estimate of the true number of events is:

$$\hat{n}(C_i) = \frac{1}{\epsilon_i} \sum_{j=1}^{n_c} n(E_j) \times P(C_i \mid E_j) \tag{2}$$

where $n(E_j)$ is the number of observed events in the j-th bin, ϵ_i is the efficiency of events in the i-th bin of the true distribution, and n_c is the number of p_T bins. In principle we have no knowledge of the initial probability $P(C_i)$ so the unfolding procedure has to be iterative and consists of the following steps: *i*) choose the initial distribution $P_o(C_i)$ from the best knowledge of the process under study or use a uniform distribution. Hence, the expected number of

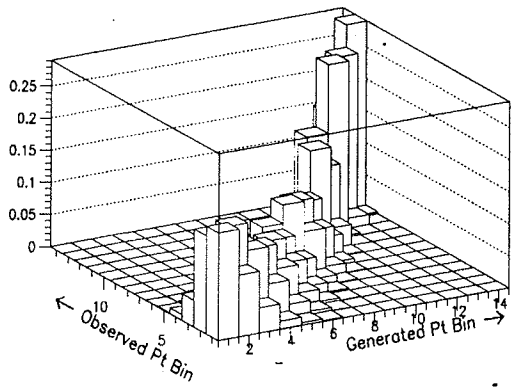

FIG. 7. Matrix $P(E_j \mid C_i)$ used to unfold $d\sigma/dp_T$ distribution of the $W \rightarrow e\nu$ data. The data from the range $0 - 200$ GeV/c has been binned in 14 bins: five 3 GeV/c bins in $(0 - 15)$ GeV/c range; three 5 GeV/c bins in $(15 - 30)$ GeV/c range; two 10 GeV/c bins in $(30 - 50)$ GeV/c range; two 25 GeV/c bins in $(50 - 100)$ Gev/c range; single 40 GeV/c bin for $(100 - 140)$ GeV/c range; and single 60 GeV/c bin for $(140 - 200)$ GeV/c range.

events is $\hat{n}_o(C_i) = P_o(C_i)N_{obs}$; *ii*) calculate the expected number of events $\hat{n}(C_i)$ and $P(C_i)$ from eq. 2; *iii*) make χ^2 comparison between $\hat{n}_o(C_i)$ and $\hat{n}(C_i)$; *iv*) replace $P_o(C_i)$ by $P(C_i)$ and $\hat{n}_o(C_i)$ by $\hat{n}(C_i)$ and start again. The iterations are stopped when the value of the χ^2 is "small enough". The number of iterations, or alternatively the value of χ^2, is optimized using Monte Carlo data.

The performance of this technique has been studied on Monte Carlo data by unfolding a hundred statistically independent $W \rightarrow e\nu$ data samples of the same magnitude as the available data set. The utilized smearing matrix $P(E_j \mid C_i)$ is shown in Fig. 7. The input p_T distribution to be unfolded was taken from reference (4). The average unfolded distribution is compared to the original in Fig. 8.

MEASUREMENT UNCERTAINTIES

The transverse momentum of the W boson is measured from the hadronic recoil of the W, while the Z boson p_T is obtained from the sum of two electron transverse momenta. Thus systematic uncertainities of $W \rightarrow e\nu$ differential cross section come from uncertainties of: *i*) hadronic energy scale, *ii*) underlying event contribution, *iii*) hadronic resolution, and *iv*) background shape and magnitude in the modeling used to produce the smearing matrix $P(E_j \mid C_i)$. The hadronic energy scale is determined by balancing the Z boson p_T determined from the hadronic recoil and from the transverse momenta of the two

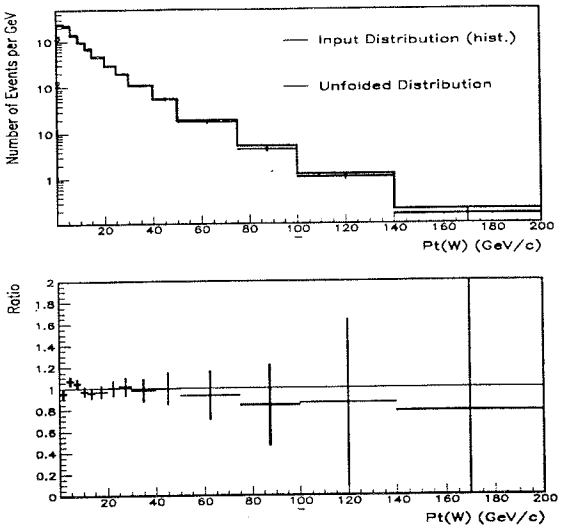

FIG. 8. Comparison of mean unfolded (crosses) and input (solid histogram) distributions (top) and the ratio of the two distributions (bottom).

electrons along the bisector of the angle subtended by the two. The uncertainty on the hadronic scale is thus controlled by the number of observed Z candidates and for this data sample it produces $\approx$ 20% uncertainty in the measurement. The magnitude of the underlying event contribution is also obtained from the Z sample by matching the Z boson p_T resolution between data and Monte Carlo and has been estimated to be of the order of 10% for this measurement. The uncertainty of the background shape and the magnitude is small at low and medium p_T's but dominates at high p_T values. The statistical uncertainty for this sample is of the order of 5% per bin (high momentum bins have larger uncertainty in the range (10 - 30)%). We thus see that the measurement uncertainty of the W boson $d\sigma/dp_T$ is completely dominated by systematic effects, most of which are directly controlled by the number of observed Z bosons.

The statistical uncertainty for the Z boson $d\sigma/dp_T$ measurement is of the order of $(10 - 20)$% up to 70 GeV/c. The systematic uncertainities of the Z boson transverse momentum measurement come from the uncertainty of: *i*) electron energy scale, *ii*) electron energy resolution, and *iii*) uncertainty of the angular resolutions. At the current level of the Z boson statistics neither of the above mentioned systematic uncertainities are particularly large.

The current W and Z boson samples collected by CDF and DØ are steadily increasing and by the end of the 1994-95 collider run the data samples will be an order of magnitude larger per experiment than the above discussed sample. Fig. 9 and Fig. 10 show the p_T distributions of $W \rightarrow e\nu$ and $Z \rightarrow e^+e^-$ for a 72.9 pb^{-1} CDF data sample accumulated during the 1993-93 run and part of

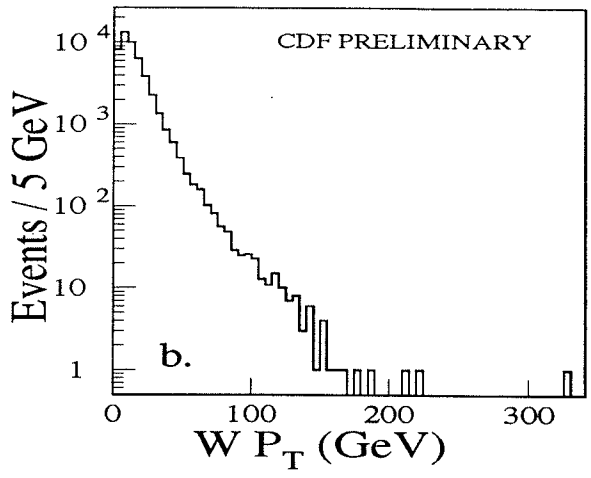

FIG. 9. p_T distribution for $W \to e\nu$ for 72.9 pb^{-1} of data collected by the CDF collaboration.

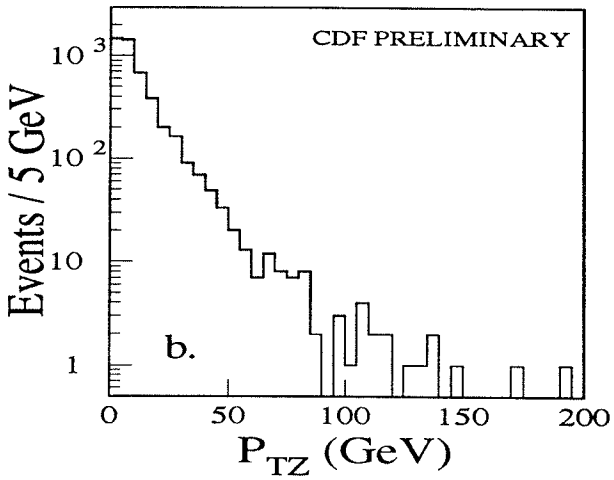

FIG. 10. p_T distribution for $Z \to e^+e^-$ for 72.9 pb^{-1} of data collected by the CDF collaboration.

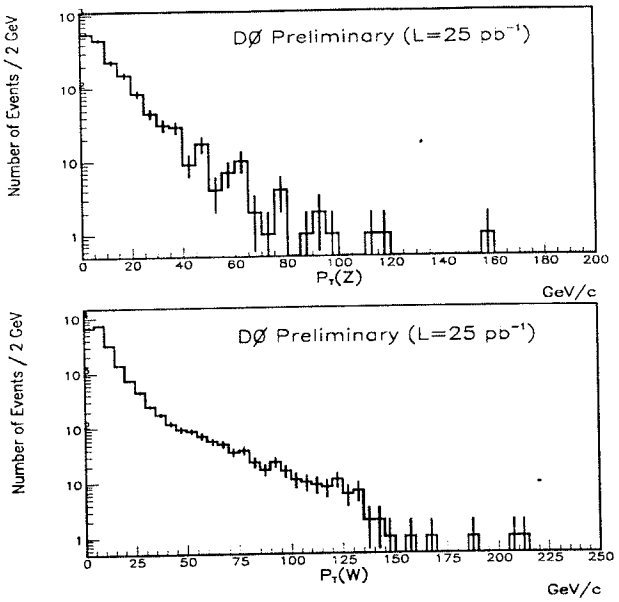

FIG. 11. p_T distributions of the $Z \to e^+e^-$ (top) and $W \to e\nu$ (bottom) for the 25 pb^{-1} data sample collected by DØ collaboration.

the 1994-95 run. Fig. 11 shows W and Z p_T distributions for 25 pb^{-1} of DØ data accumulated during part of the 1994-95 run.

The large increase in the number of observed Z boson decays will help to significantly reduce the systematic uncertainty of the W boson p_T measurement as well as directly improve the knowledge of Z p_T.

CONCLUSION

The W and Z boson differential cross section $d\sigma/dp_T$ measurements have been examined and the major sources of measurement uncertainty identified. The largest contributors to the W boson differential cross section uncertainty are the hadronic energy scale uncertainty, and underlying event modeling, with background subtraction dominating only at very high transverse momentum values. The uncertainty of the Z boson differential cross section is dominated by the statistical error.

Unfolding detector smearing with a method based on Bayes' theorem has been discussed and its satisfactory performance demonstrated in the case of W boson.

We are grateful to the DØ and CDF Collaborations for discussions of their data.

REFERENCES

1. J.Collins, D.Soper and G.Sterman, Nucl.Phys. **B 250**, 199 (1985); J.Collins and D.Soper, Nucl.Phys. **B 193**, 381 (1981); bf B 213, 545(E) (1983); **B 197**, 446 (1982).
2. C.Davies, B.Webber and W.J.Stirling, Nucl. Phys. **B 256**, 413 (1985); C.Davies and W.J.Stirling, Nucl. Phys. **B 244**, 337 (1984); C.Davies, Ph.D. Thesis, Churchill Collage (1984).
3. G.Altarelli, R.K.Ellis, M.Greco and G.Martinelli, Nucl. Phys. **B 246**, 12 (1984).
4. P.B.Arnold, R.Kauffman, Nucl. Phys. **B 349**, 381 (1991).
5. G.A.Ladinsky, C.P.Yuan, Phys. Rev. **D 50** 4239 (1994);
6. P.B.Arnold, M.H.Reno, Nucl. Phys.**B 319**, 37 (1989);
   R.J.Gonsalves, J.Pawlowski, C-F.Wai Phys Rev. **D 40**, 2245 (1989).
7. J.Alitti *et al.*, Z.Phys. **C 47**, 523 (1990); C.Albajar *et al.*, Z.Phys. **C 44**, 15 (1989).
8. F. Abe, *et al.*, Phys. Rev. Lett. **66**, 2951 (1991); B.L. Winer, Ph.D. Thesis (1991) Lawrence Berkeley Laboratory preprint LBL-30221; F.Abe,*et al.*, Phys. Rev. Lett. **67** 2937 (1991); J.S.T. Ng, Ph.D. Thesis (1991), Harvard University preprint HUHEPL-12.
9. S.Abachi, *et al.* (DØ Collaboration), Nucl. Instr. Meth. **A 338**, 185 (1994);
10. H.Aihara, *et al.* (DØ Collaboration), Nucl. Instr. Meth. **A 325**, 393 (1993);
11. S.Abachi, *et al.* (DØ Collaboration), Nucl. Instr. Meth. **A 324**, 53 (1993);
12. J. Z-Y. Jiang, Ph.D. Thesis, State University of New York at Stony Brook, (1995).
13. G.D'Agostini, DESY report, DESY 94-099 (1994).